Available online at www.sciencedirect.com
SCIENCE DIRECT
Catalysis Today 105 (2005) 122–133
CATALYSIS TODAY
www.elsevier.com/locate/cattod

DFT calculations of EPR parameters of transition metal complexes: Implications for catalysis

Alexander C. Saladino, Sarah C. Larsen *

Department of Chemistry, University of Iowa, Iowa City, IA 52242, USA

Abstract

Transition metal and ligand hyperfine coupling constants for paramagnetic vanadium and copper model complexes have been calculated using DFT methods that are available in commercial software packages. Variations in EPR parameters with ligand identity and ligand orientation are two of the trends that have been investigated with DFT calculations. For example, the systematic variation of the vanadium hyperfine coupling constant with orientation for an imidazole ligand in a VO^{2+} complex has been observed experimentally and has also been reproduced by DFT calculations. Similarly, changes in the vanadium hyperfine coupling constant with ligand binding have been calculated using model complexes and DFT methods. DFT methods were also used to calculate ligand hyperfine coupling constants in transition metal systems. The variation of the proton hyperfine coupling constant with water ligand orientation was investigated for $[VO(H_2O)_5]^{2+}$ and the results were used to interpret high resolution EPR data of VO^{2+}-exchanged zeolites. Nitrogen hyperfine and quadrupole coupling constants for VO^{2+} model complexes were calculated and compared with experimental data. The computational results were used to enhance the interpretation of the EPR data for vanadium-exchanged zeolites which are promising catalytic materials. The implications of the DFT calculations of EPR parameters with respect to catalysis will be discussed.

Keywords: Density functional theory (DFT); Electron Paramagnetic resonance (EPR)

1. Introduction

Electron paramagnetic resonance (EPR) spectroscopy is a valuable spectroscopic tool for investigating the electronic environment of paramagnetic transition metals, such as vanadium(IV) and copper(II). These transition metals have an important role in catalytic systems such as transition metal-exchanged zeolites. The EPR parameters, such as the electronic g tensor, and the hyperfine coupling constant or A tensor, reflect the coordination environment of the transition metal ion [1–3]. The hyperfine coupling constants and g values depend on the ligand field surrounding the transition metal ion and ligand field theory (LFT) has been used to relate electronic structure to the measured EPR parameters [4–7]. For transition metals such as Cu^{2+}, the spin orbit interaction contributes significantly to the hyperfine coupling constant [4–6]. LFT has been widely used to relate the spin orbit coupling contribution to the hyperfine interaction and the g-shifts [4–6,8].

Recent advances in computational chemistry have lead to the development of new quantum chemical methods based on density functional theory (DFT) for electronic structure calculations of EPR parameters, such as g and A tensors. Several groups have reported computational methods for calculating g tensors [9–15]. The relativistic methods for calculation of g and A values developed by van Lenthe have been incorporated into a commercial software package, Amsterdam Density Functional Theory (ADF 2002.01) [16–18], which uses Slater type orbitals (STO's) [19]. Recently, the relativistic DFT methods of van Lenthe have been applied to the calculation of EPR parameters for transition metal complexes [20–22]. Another DFT method for calculating A tensors has been incorporated into Gaussian98 software [23]. This method does not include relativistic effects or spin orbit coupling and uses Gaussian type orbitals (GTO's) [24].

* Corresponding author. Tel.: +1 31 9335 1346; fax: +1 31 9335 1270.
E-mail address: sarah-larsen@uiowa.edu (S.C. Larsen).

0920-5861/$ – see front matter © 2005 Elsevier B.V. All rights reserved.
doi:10.1016/j.cattod.2005.04.018

Kaupp and co-workers have published several papers evaluating the use of Gaussian98 for nonrelativistic calculations of *A* tensors for transition metal systems [25–27]. Also, Barone has calculated EPR hyperfine coupling constants using these same methods incorporated in Gaussian for organic pi-radicals [28]. The basic theory behind EPR hyperfine coupling constant calculations can be found in many different books [6,7].

In this paper, several examples of the use of DFT calculations to interpret EPR data for transition metal complexes will be presented. Vanadium and copper *g* and *A* tensor calculations for a series of vanadium and copper complexes will be reviewed. In many cases, complexes were chosen which had readily available EPR experimental data so that the accuracy of the computational methods could be assessed. The relativistic methods of van Lenthe as incorporated into the ADF program were used to calculate the *g* and *A* tensors for each of the complexes. In addition, the *A* tensors were also calculated using nonrelativistic methods as incorporated into Gaussian98. A comparison of the performance of these relativistic and nonrelativistic methods for calculation of *A* tensors of transition metal complexes will be made. Examples of DFT calculations of ligand hyperfine and quadrupole coupling constants for transition metal complexes will also be presented. The overall efficacy of using DFT methods to calculate EPR parameters of transition metal complexes will be discussed as will the limitations of current DFT methods. The implications for modeling catalytic systems using DFT calculations of EPR parameters will be presented.

2. Computational methods

2.1. Calculations with ADF

The ADF program package (ADF 2002.01) [16–18] was used to calculate the *g* and *A* tensors for each of the transition metal complexes. The methods for calculating *g* and *A* tensors were developed by van Lenthe et al. [13,14,22] and are implemented in ADF software. Two approaches can be used for *A* tensor calculations with ADF: the scalar-relativistic spin-unrestricted open shell Kohn–Sham (SR UKS) calculation and the spin orbit coupling and scalar-relativistic spin-restricted open shell Kohn–Sham (SO + SR ROKS) calculation. In the SR UKS method, spin orbit coupling is not included, but spin polarization effects are included making this the preferred method for calculating isotropic hyperfine coupling constants (A_{iso}). In the SO + SR ROKS method, spin orbit coupling effects are included, but not spin polarization effects. The SO + SR ROKS method is used for calculating *g* tensors and the anisotropic contribution to the hyperfine coupling constants (A_D). In the most recent version of ADF (2004.1), the implementation of a scalar-relativistic spin-unrestricted calculation (SO + SR UKS) with spin orbit coupling effects was introduced for *g* and *A* value calculations.

Three different combinations of exchange and correlation potentials were used in the *g* and *A* tensor calculations: BLYP, BP86, and BPW91. BLYP uses the pure-exchange electron gas formula as the local density approximation (LDA) with Becke gradient correction [29] for exchange and Lee, Yang, and Parr correction for correlation added [30,31]. Both BP86 and BPW91 use the parameterized electron gas data given by Vosko et al. for the LDA [32] with the Becke gradient correction for exchange. BP86 uses the correlation correction by Perdew [33] while BPW91 used the correlation correction by Perdew–Wang [34–36]. The basis set TZ2P was used for all calculations and all atoms [18,37–39]. The basis set TZ2P is a double ζ Slater type orbital (STO) in the core and triple ζ in the valence shell with two polarization functions.

2.2. Calculations with Gaussian

All-electron unrestricted Kohn–Sham calculations of hyperfine tensors were conducted using Gaussian98 A11.3 [23]. Relativistic effects and spin orbit contributions were not included in the Gaussian98 calculations. However, Gaussian98 provides a much wider choice of exchange and correlation functionals and basis sets than ADF. Nine different density functionals were used in the Gaussian98 calculations: BLYP, B3LYP, BHLYP, BP86, B3HP86, BHP86, BPW91, B3PW91, and BHPW91. The first three functionals are a combination of the LYP [30,31] correlation functional with the Becke (B) [29], the Becke three parameter (B3) [40] and the Becke half and half (BH) [41] exchange functionals. The next three functionals are a combination of the P86 [33] correlation functional with the B, B3, and BH exchange functionals, respectively. The last three functionals are a combination of the PW91 [34–36] correlation functional with the B, B3, and BH exchange functionals, respectively. A 15s11p6d/9s7p4d basis set from

Table 1
Features of selected DFT software packages for calculations of EPR parameters

Program	EPR parameters	Basis sets[a]	Exchange and correlation functionals	Relativistic effects[b]	Spin
ADF2000.02	*g*	STO	BP86, BLYP, BPW91	Spin orbit (SO + SR)	Restricted (ROKS)
ADF2000.02	*A*	STO	BP86, BLYP, BPW91	Scalar (SR)	Unrestricted (UKS)
ADF2004.01	*A*, *g*	STO	BP86, BLYP, BPW91	Spin orbit, scalar (SO + SR)	Unrestricted (UKS)
Gaussian98	*A*	GTO	Gradient corrected and hybrid functionals	No	Unrestricted

[a] STO: Slater type orbitals, GTO: Gaussian type orbitals.
[b] Incorporated using the zeroth order regular approximation (ZORA).

Kaupp et al. was used, which is the double ζ (DZ) basis set [42] with the most diffuse function of Dolg added (1s,2p,1d) [26]. The SCF convergence criterion was set to 10^{-6} in RMS DM and 10^{-4} in MAX DM.

2.3. Comparison of DFT methods

A comparison of the main features of the DFT methods used to calculate EPR parameters in this paper are listed in Table 1. ADF provides several methods for calculating g and A values. The most recent improvement (in ADF 2004) involves the calculation of both g and A values in a spin-unrestricted calculation with spin orbit effects included. To date, all Gaussian calculations of A values are nonrelativistic. However, gradient corrected and hybrid functionals can be used in Gaussian for calculations of A values and these cannot currently be used in ADF g and A calculations.

3. DFT calculations of transition metal hyperfine coupling constants

3.1. Vanadium hyperfine coupling constant calculations for model complexes

VO^{2+} complexes for which the crystal structures and EPR parameters are known were used as model compounds to evaluate the computational methods for calculating EPR parameters. Calculations of the EPR parameters were conducted using different computational methods for a series VO^{2+} complexes including $[VO(H_2O)_5]^{2+}$, $VO(Ma)_2$, $VO(Acac)_2$, $[VO(Mal)_2]^{2-}$, $[VO(Ox)_2]^{2-}$, and $VO(Gly)_2$ [43]. Each of the VO^{2+} complexes studied has a d^1 electronic configuration with one unpaired electron. The vanadium electron nuclear hyperfine interaction is characterized by an interaction between the unpaired electron (S = 1/2) and the vanadium nuclear spin (I = 7/2, 99.8% natural abundance). Two interactions contribute to the vanadium hyperfine coupling tensor: an isotropic or Fermi contact interaction, A_{iso}, and an anisotropic or dipolar hyperfine interaction, A_D [7]. A_{iso} and A_D can be calculated from the principal values of the A tensor using the following equations:

$$A_{iso} = \frac{A_{11} + A_{22} + A_{33}}{3} \quad (1)$$

$$A_{D,x} = A_{11} - A_{iso}$$

$$A_{D,y} = A_{22} - A_{iso}$$

$$A_{D,z} = A_{33} - A_{iso}$$

The isotropic hyperfine interaction, A_{iso}, is related to the spin density at the magnetic nucleus, and therefore, inclusion of spin polarization effects is particularly important for accurate calculations of A_{iso} [22,25].

The A_{iso} values were calculated for the VO^{2+} complexes using Gaussian98 and nine different functionals and using ADF and three different functionals. The complete set of data for all of the complexes can be found in reference [43]. DFT results for a representative complex $[VO(acac)_2]$ are shown in Figs. 1 and 2 with the solid black bars representing Gaussian results, the solid white bars representing ADF results and the light gray shaded bar indicating experimental data. The A_{iso} values calculated for $[VO(acac)_2]$ using ADF (SR UKS, GGA functionals) are approximately 70% of the experimental value of −307 MHz. This is not surprising since GGA functionals have been previously shown to underestimate the spin-polarization of the s-type metal core orbitals [26,27]. Similar results are observed for A_{iso} calculations with Gaussian and GGA functionals indicating that the two methods perform similarly with the same

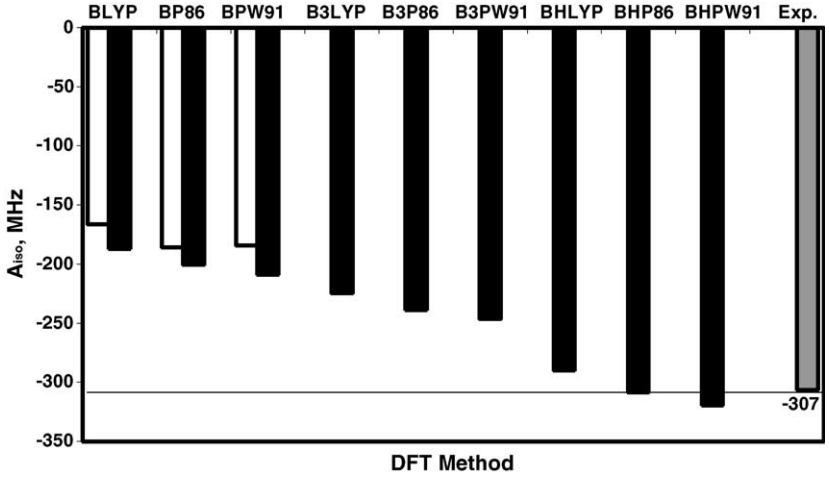

Fig. 1. Comparison of calculated A_{iso} values in MHz for $[VO(acac)_2]$ using data in reference [43]. The solid black bars represent the A_{iso} values from the Gaussian98 calculations with the different functionals listed, the solid white bars represent the A_{iso} values from the ADF (SR UKS) calculations with the functionals listed, and the dotted bar represents the experimentally measured A_{iso}.

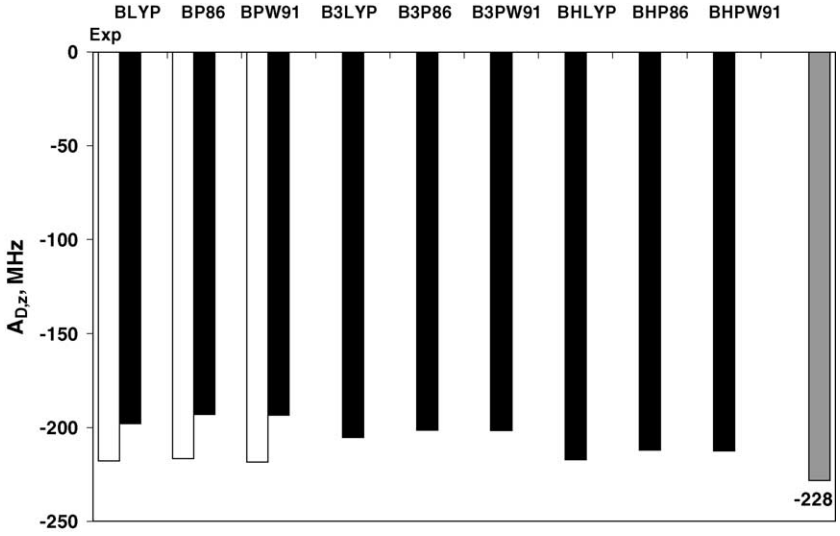

Fig. 2. Comparison of calculated $A_{D,z}$ values in MHz for [VO(acac)$_2$] using data in reference [43]. The solid black bars represent the $A_{D,z}$ values from the Gaussian98 calculations with the different functionals listed, the solid white bars represent the $A_{D,z}$ values from the ADF (SO + SR ROKS) calculations with the functionals listed, and the dotted bar represents the experimentally measured $A_{D,z}$.

functional. Overall, the Gaussian DFT calculations of A_{iso} with the hybrid functionals (BHLYP, BHP86, and BHPW91) exhibit the best agreement with experimental results. As can be seen in Fig. 1, the A_{iso} value calculated with the BHP86 functional provides the best quantitative agreement with the experimental data.

The DFT results for $A_{D,z}$ for [VO(acac)$_2$] are presented in Fig. 2. The plotted ADF values were calculated using the SO + SR ROKS method (solid white bars) and provide the best quantitative agreement with experimental results relative to the SR UKS method (not shown). The A_D values calculated for [VO(acac)$_2$] using Gaussian98 (solid black bars) are also quite close to the experimental results (~85–95% of experimental value) and are much less sensitive to the choice of functional than the corresponding A_{iso} calculations. Similar agreement is observed for $A_{D,x}$ and $A_{D,y}$.

These results indicate that for A tensor calculations with Gaussian98, the best agreement with experimental data is obtained using the hybrid functionals, BHLYP, BHPW91, and BHP86. This is in agreement with previous studies by Munzarova and Kaupp who observed that the calculated A_{iso} value for transition metal complexes is dependent on the functional [26]. This has previously been observed for organic pi-radicals [28]. For A_{iso} value calculations of vanadium(IV) complexes using Gaussian98, Munzarova and Kaupp found that the best quantitative agreement with experimental data was found for the hybrid functional, BHPW91, due to the mixing of exact exchange with the hybrid functional which enhances the spin polarization of s-type metal core orbitals relative to GGA functional [26]. The same general trends in calculated values were observed for all of the VO^{2+} complexes examined as previously suggested by Kaupp who pointed out that the deficiencies in density functionals are systematic for complexes of related electronic structure [25].

3.2. Orientation dependence of the vanadium hyperfine coupling constants for imidazole ligands in vanadyl imidazole complexes

The EPR spectra of VO^{2+} complexes (square planar or octahedral geometry) in which different equatorial ligands are present can often be interpreted using an empirical additivity relationship [1]. The additivity relationship for equatorial ligands in VO^{2+} complexes is given by the equation below:

$$A = \sum_i n_i A_i \quad (2)$$

where n_i = number of equatorial ligands of type i, A_i = contribution to A from each equatorial ligand of type i.

The additivity relationship can be used to calculate the vanadium hyperfine coupling constant, A, for a VO^{2+} complex when the number of equatorial ligands and the A_i values for each of the equatorial ligands are known.

In a recent study, Pecoraro and co-workers reported the use of the additivity relationship to predict the orientation of equatorial imidazole rings relative to the VO^{2+} bond in VO^{2+} model complexes [44]. Prior to Pecoraro's study, Cornman et al. [45], Chasteen [1] and van Willigen and co-workers [46] had each published different values for $A_{||}$(imidazole) that were used in the context of the additivity relationship to interpret the EPR spectra of VO^{2+} complexes with equatorial imidazole ligands. The results of Pecoraro's study suggested that the differences in additivity relationship values for the coordinated imidazole could be due to different orientations of the imidazole ring relative to the equatorial plane.

In Pecoraro's study, five new VO^{2+} imidazole model complexes with the imidazole rings in different orientations with respect to the VO^{2+} bond were synthesized [44]. They found that $A_{||}$ (imidazole contribution) varied from 120 to 138 MHz for parallel and perpendicular bound imidazole ligands, respectively. Their data could be fit to the following functional form: $A_{||}(\text{imid}) = A + B\sin(2\theta - 90)$ where A and B are fitted parameters equal to 128 and 9 MHz, respectively.

In our study, the dependence of the vanadium hyperfine coupling constant on ligand orientation was investigated using DFT methods [47]. A model complex, $[VO(imid)(H_2O)_4]^{2+}$, was constructed and optimized so that the effect of imidazole ligand orientation on vanadium hyperfine coupling constant could be investigated using DFT calculations. The dihedral angle, θ, that characterizes the orientation of the imidazole ring relative to the V=O bond was varied from 0° to 345°. For each value of the dihedral angle, the vanadium hyperfine coupling constant, A, was calculated using the relativistic methods of van Lenthe et al. [13]. The A values were calculated using two different methods, the SR UKS method (A_{iso}) and the SO + SR ROKS method (A_D). The most accurate A values for transition metals when spin orbit effects are small are currently obtained by combining A_{iso} values calculated using the SR UKS method and A_D calculated using the SO + SR ROKS method. The principal values of the A tensors for the $[VO(imid)(H_2O)_4]^{2+}$ complexes were calculated with the different methods and as a function of the dihedral angle. The combined A_{33} value (or $A_{||}$ value assuming axial symmetry) versus the dihedral angle is plotted in Fig. 3. The calculated vanadium $A_{||}$ values vary systematically with dihedral angle.

A least squares fit of the calculated vanadium $A_{||}$ values for the $[VO(imid)(H_2O)_4]^{2+}$ model complex to the functional form, $A_{||} = A + B\sin(2\theta - 90)$ yields fitted parameters, $A = -423$ and $B = -6.7$ MHz where The value of -423 MHz corresponds to the average $A_{||}$ value for $[VO(imid)(H_2O)_4]^{2+}$. The fitted line is the solid line in Fig. 3.

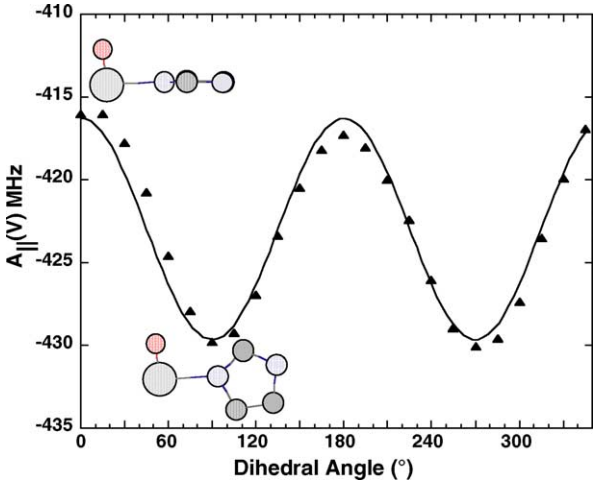

Fig. 3. The calculated vanadium hyperfine coupling constant ($A_{||}$) for $[VO(imid)(H_2O)_4]^{2+}$ as a function of the dihedral angle, θ, is plotted. $A_{||}$ was calculated from A_{iso} (SR UKS, BP86) + A_D (SR + SO ROKS, BP86). The data was fit to $A_{||} = A + B(\sin 2\theta - 90)$ where $A = -423$ MHz and $B = -6.7$ MHz. Adapted with permission from [47], Copyright 2002 American Chemical Society.

The theoretical basis for the orientation dependence of the vanadium hyperfine coupling constant is the overlap between the unpaired electron in the vanadium d_{xy} orbital and the aromatic p orbital of the coordinated imidazole nitrogen [47]. As the imidazole ring is rotated from a dihedral angle of 0° to 90°, the overlap between the aromatic p orbital and the vanadium d_{xy} orbital decreases leading to a decrease in the hyperfine coupling constant. Computationally, this was explained by examining the contributions of the d_{xy} and aromatic p orbital to the singly occupied molecular orbital (SOMO), which trended accordingly [47].

3.3. Copper hyperfine coupling constants and the effect of spin orbit coupling

Relativistic DFT calculations of the transition metal hyperfine coupling constant for a series of copper square planar complexes, including $Cu(Quin)_2$, $Cu(Acac)_2$, $Cu(L\text{-}AlaO)_2$, and $[Cu(Ox)_2]^{2-}$ have been conducted [48]. The Cu^{2+} has a d^9 electronic configuration (S = 1/2) and a copper nuclear spin of 3/2 (^{63}Cu, ^{65}Cu, 69.1 and 30.9% natural abundance, respectively). In contrast to vanadium, the spin orbit coupling contributions to the copper hyperfine coupling constant are substantial. The calculations of the EPR parameters for the Cu^{2+} complexes were conducted

Table 2
Relativistic (ADF) calculated and experimental isotropic and dipolar hyperfine coupling constants for copper model complexes[a]

		BP86 (SR UKS)	BP86 (SO + SR UKS)	Exp.[b]
[Cu(quin)]	A_{iso}	−214	−129	−238[c]
	$A_{D,x}$	221	133	132
	$A_{D,y}$	164	167	132
	$A_{D,z}$	−386	−300	−263
$[Cu(ox)_2]^{2-}$	A_{iso}	−228	−145	−180[d]
	$A_{D,x}$	189	146	156
	$A_{D,y}$	191	147	156
	$A_{D,z}$	−380	−292	−312
$Cu(acac)_2$	A_{iso}	−225	−141	−231[e]
	$A_{D,x}$	192	149	146
	$A_{D,y}$	197	148	146
	$A_{D,z}$	−388	−296	−292
$Cu(L\text{-}ala)_2$	A_{iso}	−206	−130	−222[f]
	$A_{D,x}$	162	155	132
	$A_{D,y}$	201	130	132
	$A_{D,z}$	−363	−285	−264

[a] All A values are given in MHz.
[b] A negative value for A_{iso} has been assumed for the experimental value for comparison with calculated values.
[c] Reference [108].
[d] Reference [109].
[e] Reference [110].
[f] Reference [111].

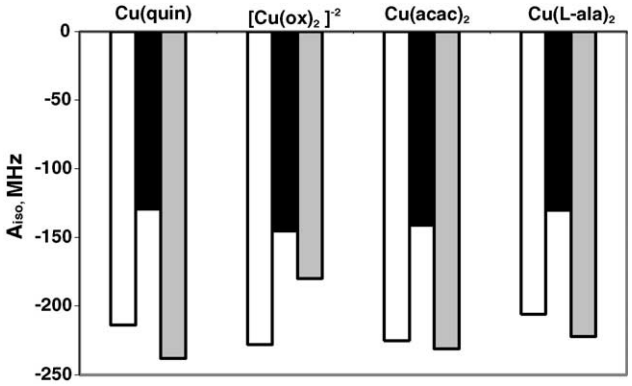

Fig. 4. Comparison of calculated A_{iso} values in MHz for copper complexes. The solid white bars represent the A_{iso} values from the ADF SR UKS (BP86) [48], the solid black bars represent the A_{iso} values from the ADF SO + SR UKS (BP86) calculations with the functionals listed, and the light gray shaded bar represents the experimentally measured $A_{D,z}$.

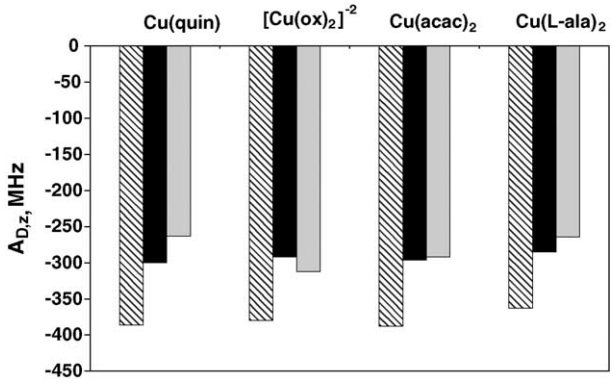

Fig. 5. Comparison of calculated $A_{D,z}$ values in MHz for copper complexes. The solid white bars represent the $A_{D,z}$ values from the ADF SR UKS (BP86) [48], the solid black bars represent the $A_{D,z}$ values from the ADF SO + SR UKS (BP86) calculations with the functionals listed, and the light gray shaded bar represents the experimentally measured $A_{D,z}$.

using different computational methods so that the relative contributions of spin polarization and spin orbit coupling to the hyperfine tensors could be evaluated. Two relativistic methods for calculating the A tensors for Cu^{2+} complexes were compared: the SR UKS method and the SO + SR UKS method. This comparison was not done in our previous study [48] since it was completed before the SO + SR UKS method was implemented in ADF. The results are listed in Table 2.

As shown in Fig. 4, the A_{iso} values calculated for Cu^{2+} complexes with the pure generalized gradient correction (GGA) functionals with the SR UKS method (solid white bars) are in relatively good agreement with the experimental values (gray shaded bars), with an average deviation of 11%. However, the good agreement observed in this study for the A_{iso} for the copper complexes is most likely due to a cancellation of errors. This conclusion can be tested by comparing the A_{iso} values (SR UKS) with the A_{iso} values calculated with spin orbit coupling effects included in the SO + SR UKS method (solid black bars).

The comparison of these results suggests that the spin orbit coupling contribution to A_{iso} for these copper complexes is large (~80–100 MHz) and positive, and therefore, will have a substantial impact on the calculated A_{iso} values. A similar analysis of spin orbit coupling contributions to A_{iso} for nickel complexes has been previously utilized [22]. The exclusion of spin orbit coupling effects (approximately, +80–100 MHz) in the SR UKS calculation offsets the underestimation of core shell spin polarization that has been observed previously [15,26,27] when using GGA functionals. This cancellation of errors in the A_{iso} calculations, results in the fortuitous agreement of the calculated (SR UKS) and experimental copper A_{iso} values.

Therefore, we can conclude that better computational results would be obtained if a more accurate description of core shell spin polarization through different functionals were available [15,22]. Recently, Neese also addressed this problem with a new method for calculating transition metal hyperfine coupling constants in an unrestricted DFT calculation with the inclusion of spin orbit coupling effects [15]. Although this new method significantly improved the A tensor calculations, Neese concluded that more accurate functionals are still needed to further improve DFT calculations of spin dependent properties [15].

The DFT calculations of A_D are sensitive to spin orbit coupling effects but not very sensitive to spin polarization effects as illustrated by the results graphed in Fig. 5. The solid black bars show the SO + SR UKS method and the light gray shaded bars indicate the experimental values for A_{dz}. The solid white bars represent the SR UKS results and these calculations are not as accurate as SO + SR UKS since spin orbit coupling is not included. Quantitatively, very good results were obtained using the new SO + SR UKS method.

4. DFT calculations of ligand hyperfine and quadrupole coupling constants for transition metal complexes

4.1. Orientation dependence of proton hyperfine coupling constants in $VO(H_2O)_5^{2+}$

DFT methods can also be used to calculate hyperfine coupling constants for ligands in transition metal complexes. Experimentally, ligand hyperfine coupling constants that are too small to be resolved in CW EPR experiments are measured using electron nuclear double resonance (ENDOR) or electron spin echo envelope modulation (ESEEM) techniques [46,49–56]. In this example, proton hyperfine coupling constants for the vanadium complex $[VO(H_2O)_5]^{2+}$ were calculated using DFT methods [57]. Single crystal ENDOR data for the proton hyperfine coupling constants of $[VO(H_2O)_5]^{2+}$are available for comparison with the calculated values [58].

In the DFT study, the $[VO(H_2O)_5]^{2+}$ complex was geometry optimized and then an SR UKS DFT calculation of

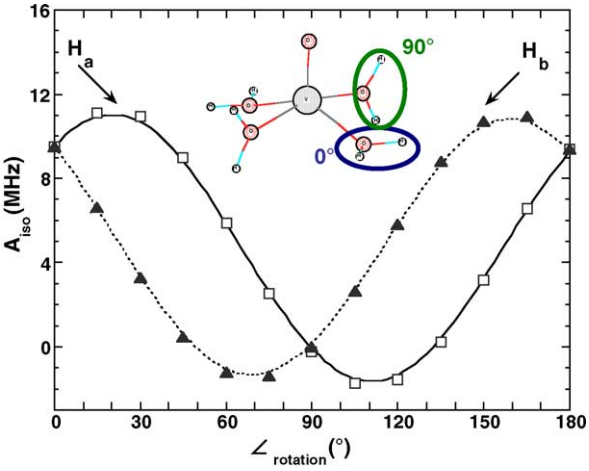

Fig. 6. Calculated proton hyperfine coupling constants, A_{iso}, plotted vs. the angle of rotation of an equatorial water molecule in $[VO(H_2O)_5]^{2+}$ relative to the equatorial plane. The variation of A_{iso} for each proton, H_a and H_b on the water molecule is shown as a function of the rotation angle of the water molecule. Two of the possible orientations for the water molecule are illustrated schematically. Adapted with permission from [57], Copyright 2001 American Chemical Society.

the proton hyperfine coupling constants was completed [57]. Then, one of the equatorial water molecules was systematically rotated by 15° (while the other water molecules remained in their original orientations) and the SR UKS calculation was repeated for each orientation so that the proton hyperfine coupling constants of the equatorial water ligand could be mapped as a function of orientation. The proton hyperfine coupling constants, A_{iso}, for each of the two protons, H_a and H_b, on the water molecule being rotated, are graphed in Fig. 6. The proton hyperfine coupling constant is sensitive to orientation and varies from 10 to −1 MHz as a function of dihedral angle. The calculated proton hyperfine coupling constants graphed in Fig. 6 can be used to predict the orientation of an equatorial water molecule in $[VO(H_2O)_5]^{2+}$. For example, if the proton hyperfine coupling constants are equivalent and positive with a large magnitude (∼10 MHz), the DFT calculations indicate that the water molecule is oriented in or nearly in the equatorial plane. If the proton hyperfine coupling constants are equivalent and small in magnitude, the DFT calculations indicate that the water molecule is oriented perpendicular to the equatorial plane. These results can be rationalized by considering the overlap between the vanadium d_{xy} orbital and the hydrogen molecular orbitals which is maximized when the hydrogen atoms are in the equatorial plane and minimized when the hydrogen atoms are rotated out of the equatorial plane.

The DFT results can be compared with experimental single crystal ENDOR results for $[VO(H_2O)_5]^{2+}$ [58]. The single crystal results indicate that there are two groups of protons with approximately equivalent proton hyperfine coupling constants. The first four protons have A_{iso} values of −0.39, 4.08, −0.05, and 4.57 MHz. The second four protons have A_{iso} values of 8.67, 7.14, 7.73, and 6.96 MHz. The interpretation which is supported by the DFT calculations is that the first two water molecules are oriented in or nearly in the equatorial plane and the second two water molecules are located approximately perpendicular to the equatorial plane.

4.2. Nitrogen hyperfine and quadrupole coupling constants for vanadyl model complexes

Nitrogen–ligand hyperfine and quadrupole coupling constants for vanadyl model complexes were calculated using DFT methods. These model complexes for which experimental EPR data and in most cases, crystal structures, are available will serve as a testing ground for the application of DFT methods to the calculation of ligand hyperfine and quadrupole coupling constants. The nitrogen hyperfine and quadrupole coupling constants for a group of VO^{2+} complexes containing amine ($VO(gly)_2$, VO(edda)), imine ($VO(meox)_2$, VO(salen)) and isothiocyanate groups $[VO(SCN)_4]^{2-}$ were calculated using relativistic DFT calculations [59]. The results were compared with experimental data obtained from high resolution EPR measurements.

The nitrogen hyperfine and quadrupole coupling constants were calculated for the model complexes using the relativistic methods of van Lenthe as incorporated into ADF [14]. The experimental and calculated (SR UKS, BP86) nitrogen A_{iso} values for each of the vanadyl complexes are compared using the bar graph shown in Fig. 7 where the solid black bars represent the SR UKS (ADF, BP86) results and the shaded bars represent the experimental values. The agreement between the experimental and the calculated A_{iso} values is very good with deviations ranging from <1% for VO(edda) to −10% for $VO(meox)_2$ with an average deviation of −4%. The calculated nitrogen A_{iso} values vary systematically with nitrogen type from ∼−5 MHz for amine

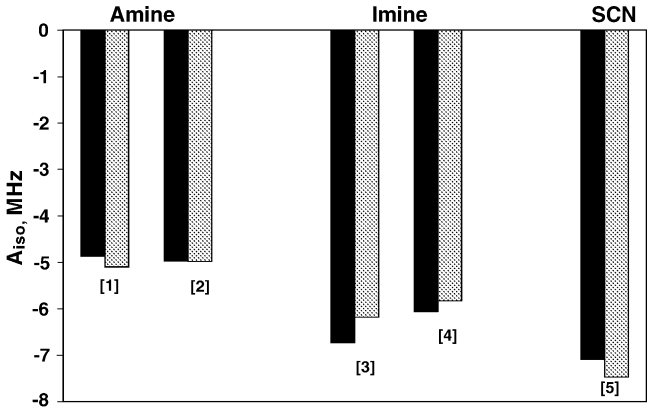

Fig. 7. The calculated nitrogen isotropic coupling constant (A_{iso}) in MHz for $VO(gly)_2$ [1], VO(edda) [2], $VO(meox)_2$ [3], VO(salen) [4], and $[VO(SCN)_4]^{2-}$ [5] as a function of the nitrogen ligand type [59]. The solid black bars represent A_{iso} values from the ADF (SR UKS, BP86) calculations and the shaded bars represent the experimentally measured A_{iso}. Reprinted with permission from [59], Copyright 2003 American Chemical Society.

complexes, to −6 to −7 MHz for imine complexes to −7 to −8 MHz for isothiocyanate complexes which reflects the experimental trend observed by Fukui et al. and LoBrutto et al. [60,61].

Both direct singly occupied molecular orbital (SOMO) and indirect spin polarization may contribute to the isotropic hyperfine coupling constant. For these vanadyl complexes, the unpaired electron on the vanadium atom occupies a d_{xy} orbital. Consequently, the overlap with the nitrogen ligand p orbitals is small, and therefore, direct spin polarization contributions are not expected to be significant. The primary contribution to the nitrogen isotropic hyperfine coupling constant is from an indirect spin transfer mechanism in which the nitrogen p orbital is polarized by an exchange interaction with the unpaired electron on the vanadium [62]. The SR UKS method includes spin polarization effects, and therefore, provides very good agreement with experimental data for the nitrogen isotropic hyperfine coupling constant as shown in the bar graph in Fig. 7. The anisotropic contributions to the hyperfine coupling constant tensor, $A_{D,x}$, $A_{D,y}$, and $A_{D,z}$ were also calculated but the quantitative agreement with experiment was not as good as for A_{iso}.

Nitrogen nuclear quadrupole coupling constants (NQCC) can be measured using ESEEM spectroscopy under conditions of *exact cancellation* [53,63–65]. *Exact cancellation* for nitrogen nuclei occurs when the nuclear Zeeman interaction and the hyperfine coupling interaction cancel in one electron spin manifold, and pure quadrupole eigenstates remain. Under conditions of exact cancellation, three pure quadrupole peaks are observed in the ^{14}N ESEEM spectrum at frequencies of $K(3+\eta)$, $K(3-\eta)$ and $2K\eta$, where K is the NQCC, $e^2qQ/4$, and η is the asymmetry parameter. The equations for the quadrupole parameters, Q_{11} and η, are given below:

$$Q_{11} = \frac{3e^2qQ}{4I(2I-1)} = \frac{3e^2qQ}{4h}$$
$$\eta = \left|\frac{Q_{33} - Q_{22}}{Q_{11}}\right| \quad (3)$$

where Q_{11}, Q_{22}, and Q_{33} are the principal values of the traceless quadrupole tensor, q is the field gradient along the principal axis of the largest field gradient (z axis) and Q is the nuclear quadrupole moment [66].

The computational results for Q_{11} are listed in Table 3 and are in good agreement with the experimental data [59]. The deviation between the calculated and experimental values ranges from 5 to 25% with an average deviation of 14%. For the amine and isothiocyanate complexes, the results were invariant with respect to the computational methods (SR UKS, SO + SR ROKS, SR ROKS). For the imine complexes, the SO + SR ROKS computational methods provided slightly better accuracy relative to the SR UKS computational method. Qualitatively, the computational results exhibit the same trend as the experimental Q_{11} values in that Q_{11} varies from amine (approximately, −1.6 MHz), to imine (approximately, −1.2 MHz) to isothiocyanate (approximately, −0.65 MHz). Warncke and co-workers recently reported a DFT computational study of the NQCC's of imidazole derivatives and the impact of the molecular environment [67].

Table 3
Calculated and experimental quadrupole coupling constants (Q_{11}) for VO_2^+ complexes with equatorially coordinated nitrogen ligands [59]

	Q_{11} (MHz)			
	SR UKS	SO + SR ROKS	SR ROKS	Experiment
$VO(gly)_2$	−1.68	−1.68	−1.68	−1.35[a]
VO(edda)	−1.62	−1.62	−1.62	−1.55[a]
$VO(meox)_2$	−1.33	−1.27	−1.27	−1.17[b]
VO(salen)	−1.30	−1.19	−1.19	−1.20[a]
	−1.24	−1.10	−1.10	−1.20[a]
$VO(NCS)_4^{2-}$	−0.65	−0.68	−0.68	−0.50[a]

[a] Reference [101].
[b] Reference [53].

5. Using DFT methods to interpret the EPR spectra of vanadium-exchanged zeolites

Vanadium-exchanged zeolites have been investigated as catalysts for use in applications, such as emission abatement reactions and oxidation reactions [2,68–72]. Vanadium-exchanged zeolites are prepared by standard ion-exchange in which vanadium(IV) or VO^{2+} replaces the charge compensating cation in the zeolite. Whittington and Anderson studied toluene oxidation on vanadium-exchanged zeolites and determined that vanadyl (VO^{2+}) groups were responsible for the catalytic activity [68]. Wark and co-workers demonstrated that vanadium-exchanged ZSM-5 (VO^{2+}-ZSM-5) is active for the selective catalytic reduction of nitric oxide with ammonia (SCR–NH_3) (Eq. (4)) [71].

$$4NO + 4NH_3 + O_2 \rightarrow 4N_2 + 6H_2O \quad (4)$$

The vanadium-exchanged zeolites were found to have catalytic activity comparable to V_2O_5/TiO_2, which is a commercial catalyst for SCR–NH_3 of NO_x in flue gases of stationary sources. The catalytic activity of VO^{2+}-ZSM-5 for SCR–NH_3 has been attributed to vanadyl (VO^{2+}) species with vanadium in the V^{4+} oxidation state [71].

EPR spectra of VO^{2+}-exchanged zeolites can be easily obtained and can be interpreted using comparisons with model complexes. The parallel components of the g and A tensors for VO^{2+} complexes are sensitive to changes in geometry and ligand binding. In fact, $g_{||}$ and $A_{||}$ for vanadium are correlated and vary systematically with ligand identification. For example, a decrease in $A_{||}$ and an increase in $g_{||}$ is observed experimentally with a change in ligand from water to ammonia [73]. The systematic variation with ligand has been well-documented using model complexes [1]. The EPR spectra for hydrated VO^{2+}-exchanged zeolites suggest that a hydrated VO^{2+} complex is present in the zeolite. After exposing the VO^{2+}-exchanged zeolite to

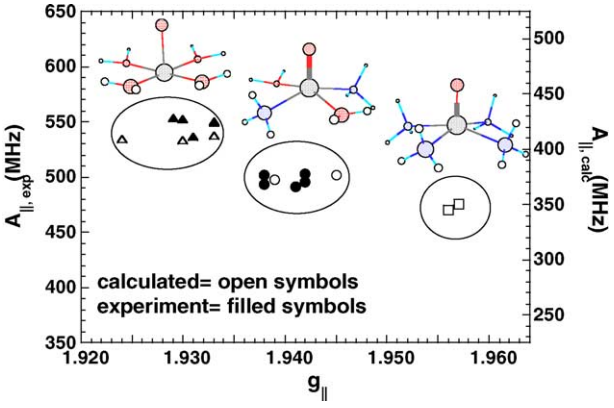

Fig. 8. Correlation plot of $A_{||}$ and $g_{||}$ showing EPR parameters of VO^{2+}-exchanged zeolites (solid symbols) before (solid triangles) and after pretreatment with ammonia (solid circles). The calculated EPR parameters for the VO^{2+} model complexes, $[VO(H_2O)_4]^{2+}$, *cis*- and *trans*-$[VO(H_2O)_2(NH_3)_2]^{2+}$, and $[VO(NH_3)_4]^{2+}$ are graphed using open triangles, circles, and squares, respectively. Adapted with permission from [73], Copyright 2001 American Chemical Society.

ammonia, the EPR parameters change and a decrease in $A_{||}$ and an increase in $g_{||}$ are observed. In this section, the EPR spectra of VO^{2+}-exchanged zeolites will be interpreted by comparing the experimental results with DFT calculations of the EPR parameters for VO^{2+} model complexes.

Several VO^{2+} model complexes, $[VO(H_2O_4)_5]^{2+}$, $[VO(NH_3)_4]^{2+}$ and *cis*- and *trans*-$[VO(NH_3)_2(H_2O)_2]^{2+}$, were constructed [73]. The structures were geometry optimized and then DFT calculations (SR UKS) of *g* and *A* values were conducted. The results are plotted in Fig. 8. The filled symbols are the experimental $g_{||}$ and $A_{||}$, values for vanadium-exchanged zeolites in the hydrated form and after adsorption of ammonia. The open symbols are the calculated $g_{||}$ and $A_{||}$, values for the model complexes shown on the graph. The calculated data has been shifted to account for the underestimation of spin polarization in the $A_{||}$ calculations. The DFT results suggest that the complex formed in the VO^{2+}-exchanged zeolites after adsorption of ammonia is actually *cis*- or *trans*-$[VO(NH_3)_2(H_2O)_2]^{2+}$, rather than $[VO(NH_3)_4]^{2+}$. Using the trends observed in the DFT calculations of the model complexes, the chemistry of the VO^{2+}-exchanged zeolites as monitored by EPR could be interpreted [73].

The vanadium ligand hyperfine coupling constants of the VO^{2+}-exchanged zeolites are too small to be resolved in the CW EPR spectrum. The unpaired electron on the vanadium is primarily in a d_{xy} orbital leading to weak overlap with the ligand orbitals and small ligand hyperfine coupling constants. Experimentally, ligand hyperfine coupling constants in VO^{2+} systems are measured by high resolution EPR techniques, such as ESEEM or ENDOR [1,74–81,51,52,54,61,82–84]. For example, ESEEM methods can be used to measure nitrogen isotropic hyperfine coupling constants (A_N) in the range of ~1–10 MHz [51,52,61]. For ligand nuclei with $I > 1/2$, the quadrupole coupling constants can also be measured and can provide additional information about the local electronic environment of the ligand [52,54,61]. Larsen and Singel measured the nitrogen hyperfine and quadrupole coupling constants for ammonia adsorbed on silica supported vanadium oxide using ESEEM spectroscopy [52]. Kevan and co-workers have used ESEEM extensively to obtain valuable distance information about coordinated ligands in transition metal-exchanged zeolites [2,85–95].

Recently, a two-dimensional ESEEM experiment, hyperfine sublevel correlation spectroscopy (HYSCORE) [96], was introduced and has been used to study a range of biological and materials systems [97–103]. The advantage of the HYSCORE experiment relative to standard ESEEM methods is that spectral assignments are simplified due to cross peaks in the two-dimensional spectrum that correlate nuclear frequencies from different electron spin manifolds, simplifying spectral assignments [104] and decreasing spectral overlap. HYSCORE spectroscopy has been used to measure the proton and nitrogen hyperfine coupling constants for hydrated VO^{2+}-exchanged zeolites and VO^{2+}-exchanged zeolites with adsorbed ammonia [105].

The HYSCORE results suggested that the hydrated vanadyl complex in the zeolite is structurally similar to $[VO(H_2O)_5]^{2+}$ and consequently, the zeolite framework does not strongly influence the hydrated vanadyl complex. Through analysis of the HYSCORE data, the orientations of the four equatorial water ligands (two water molecules oriented perpendicular and two water molecules oriented parallel relative to the equatorial plane) were determined [105]. When the hydrated vanadium-exchanged zeolite was exposed to ammonia, strong nitrogen modulation signals appeared in the HYSCORE spectra, which were analyzed to determine the nitrogen ligand hyperfine and quadrupole interactions. The results indicated that the ammonia binds in the equatorial plane with hyperfine and quadrupole coupling constants similar to those in the literature for similar complexes [51,52,61]. Importantly, the ammonia displaces water ligands indicating that the ammonia binds strongly to the vanadyl center in the zeolite which is crucial for the SCR reaction since water is a product of the reaction. The experimental HYSCORE results elucidate the structures of the hydrated vanadyl and ammonia vanadyl complexes in vanadium-exchanged zeolites. Both of these complexes are potentially important in the SCR of NO with NH_3 on vanadium-exchanged zeolites as indicated by reaction (4).

6. Implications for modeling catalysis

Transition metal and ligand hyperfine coupling constants for VO^{2+} and copper model complexes have been calculated using widely available DFT methods. The accuracy of the DFT calculations of transition metal hyperfine coupling constants is limited by the underestimation of the core spin polarization with currently available functionals [27,106,107]. Despite this shortcoming, experimentally observed

trends of EPR parameters for systems with similar electronic structures can be successfully reproduced by the DFT calculations. Variations in EPR parameters with ligand identity and ligand orientation are two of the trends that have been investigated with DFT methods. For example, the systematic variation of the vanadium hyperfine coupling constant with orientation for an imidazole ligand in a VO^{2+} complex has been observed experimentally and has also been reproduced by DFT calculations [47]. Similarly, changes in the vanadium hyperfine coupling constant with ligand binding have been calculated using model complexes and DFT methods [73]. The computational results were used to enhance the interpretation of the EPR data for vanadium-exchanged zeolites which are promising catalytic materials.

The vanadium-exchanged zeolites discussed in Section 5 have been shown to be active for the SCR of NO with NH_3. The calculations of the EPR parameters for VO^{2+} complexes were used to elucidate the structures of the hydrated vanadyl and ammonia vanadyl complexes in vanadium-exchanged zeolites. Both of these complexes are potentially important in the SCR of NO with NH_3 on vanadium-exchanged zeolites. As discussed in a previous section, the experimental HYSCORE results strongly suggest that the hydrated vanadyl complex in the zeolite is structurally similar to $[VO(H_2O)_5]^{2+}$. Through analysis of the HYSCORE data and comparison with computational results, the orientations of the four equatorial water ligands (two water molecules oriented perpendicular and two water molecules oriented parallel relative to the equatorial plane) were determined. When the hydrated vanadium-exchanged zeolite was exposed to ammonia, strong nitrogen modulation signals appeared in the HYSCORE spectra, which were analyzed to determine the nitrogen ligand hyperfine and quadrupole interactions. The results indicated that the ammonia binds in the equatorial plane with hyperfine and quadrupole coupling constants similar to those in the literature for similar complexes. Importantly, the ammonia displaces water ligands indicating that the ammonia binds strongly to the vanadyl center in the zeolite which is crucial for the SCR reaction since water is a product of the reaction. This is just one example of how the DFT calculations of EPR parameters can be used to interpret experimental data and to enhance our understanding of catalytic processes.

The accuracy of the DFT methods when calculating ligand hyperfine coupling constants in transition metal systems is improved relative to the DFT calculations of the transition metal hyperfine coupling. The variation of the proton hyperfine coupling constant with water ligand orientation was investigated for $[VO(H_2O)_5]^{2+}$ and the results were used to interpret high resolution EPR data of VO^{2+}-exchanged zeolites [57]. Nitrogen hyperfine and quadrupole coupling constants for VO^{2+} model complexes were calculated and compared with experimental data [59]. The results suggest that these DFT methods will be very useful for obtaining structural information from ligand hyperfine coupling constants for transition metal complexes.

Overall, DFT calculations of EPR parameters for transition metal complexes are emerging as a valuable tool for relating experimental EPR data to the electronic structure of transition metal complexes. Despite the shortcomings that are still problematic for DFT calculations of transition metal EPR parameters, the DFT calculations can be used to predict systematic trends that occur in the EPR parameters with ligand identity and orientation. The future is particularly bright for DFT calculations of ligand EPR hyperfine coupling constants in transition metal complexes. The DFT calculations of ligand hyperfine coupling constants in transition metal complexes show quantitatively better agreement with experimental results from high resolution EPR methods. Future improvements in the theoretical methodology for DFT calculations of EPR parameters of transition metal complexes will lead to even better agreement with experimental data and will open the door to the increased use of EPR methods for structure determination in transition metal complexes.

Acknowledgements

S.L. acknowledges support of NSF (CHE-0204847). P. Carl, M.K. Bowman and J. Woodworth are acknowledged for their contributions to this work. A portion of this research was performed in the Environmental Molecular Sciences Laboratory (a national scientific user facility sponsored by the U.S. DOE Office of Biological and Environmental Research) located at Pacific Northwest National Laboratory, operated by Battelle for DOE.

References

[1] N.D. Chasteen, in: L.J. Berliner, J. Reuben (Eds.), Biological Magnetic Resonance, vol. 3, Plenum, New York, 1981, p. 53.
[2] A.M. Prakash, L. Kevan, J. Phys. Chem. B 104 (2000) 6860–6868.
[3] J. Peisach, W.E. Blumberg, Arch. Biochem. Biophys. 165 (1974) 691–708.
[4] B.R. McGarvey, Transition Met. Chem. 3 (1966) 89.
[5] C.J. Balhausen, Introduction to Ligand Field Theory, McGraw-Hill Inc., New York, 1962.
[6] A. Abragam, B. Bleaney, Electron Paramagnetic Resonance of Transition Ions, Clarendon Press, Oxford, 1970.
[7] J.A. Weil, J.R. Bolton, J.E. Wertz, Electron Paramagnetic Resonance: Elementary Theory and Practical Applications, John Wiley & Sons Inc., New York, 1994.
[8] F. Neese, E.I. Solomon, in: J.S. Miller, M. Drillon (Eds.), Magnetism: Molecules to Materials, vol. IV, Wiley, New York, 2003.
[9] O.L. Malkina, J. Vaara, B. Schimmelpfennig, M. Munzarova, V.G. Malkin, M. Kaupp, J. Am. Chem. Soc. 122 (2000) 9206–9218.
[10] S. Patchkovskii, T. Ziegler, J. Chem. Phys. 111 (1999) 5730–5740.
[11] S. Patchkovskii, T. Ziegler, J. Am. Chem. Soc. 122 (2000) 3506–3516.
[12] G. Schreckenbach, T. Ziegler, J. Phys. Chem. A 101 (1997) 3388–3399.
[13] E. van Lenthe, P.E.S. Wormer, A. van der Avoird, J. Chem. Phys. 107 (1997) 2488–2498.

[14] E. van Lenthe, A. van der Avoird, P.E.S. Wormer, J. Chem. Phys. 108 (1998) 4783–4796.
[15] F. Neese, J. Chem. Phys. 118 (2003) 3939–3948.
[16] E.J. Baerends, J.A. Autschbach, A. Bérces, C. Bo, P.M. Boerrigter, L. Cavallo, D.P. Chong, L. Deng, R.M. Dickson, D.E. Ellis, L. Fan, T.H. Fischer, C. Fonseca Guerra, S.J.A. van Gisbergen, J.A. Groeneveld, O.V. Gritsenko, M. Grüning, F.E. Harris, P. van den Hoek, H. Jacobsen, G. van Kessel, F. Kootstra, E. van Lenthe, V.P. Osinga, S. Patchkovskii, P.H.T. Philipsen, D. Post, C.C. Pye, W. Ravenek, P. Ros, P.R.T. Schipper, G. Schreckenbach, J.G. Snijders, M. Sola, M. Swart, D. Swerhone, G. Te Velde, P. Vernooijs, L. Versluis, O. Visser, E. van Wezenbeek, G. Wiesenekker, S.K. Wolff, T.K. Woo, T. Ziegler, 2002.01 ed., SCM Amsterdam, The Netherlands, 2002.
[17] G. te Velde, F.M. Bickelhaupt, E.J. Baerends, F.C. Guerra, J.A. van Gisbergen, J.G. Snijders, T. Ziegler, J. Comp. Chem. 22 (2001) 931–967.
[18] C. Fonseca Guerra, J.G. Snijders, G. Te Velde, E.J. Baerends, Theor. Chem. Acc. 99 (1998) 391.
[19] J.C. Slater, Phys. Rev. 36 (1930) 57–64.
[20] P.J. Carl, S.L. Isley, S.C. Larsen, J. Phys. Chem. A 105 (2001) 4563–4573.
[21] E. van Lenthe, E. Baerends, J. Chem. Phys. 112 (2000) 8279.
[22] M. Stein, E. van Lenthe, E.J. Baerends, W. Lubitz, J. Phys. Chem. A 105 (2001) 416–425.
[23] M.J. Frisch, G.W. Trucks, H.B. Schlegel, G.E. Scuseria, M.A. Robb, J.R. Cheeseman, V.G. Zakrzewski, J.A. Montgomery, Jr., J. A., R.E. Stratmann, J.C. Burant, S. Dapprich, J.M. Millam, A.D. Daniels, K.N. Kudin, M.C. Strain, O. Farkas, J. Tomasi, V. Barone, M. Cossi, R. Cammi, B. Mennucci, C. Pomelli, C. Adamo, S. Clifford, J. Ochterski, G.A. Petersson, P.Y. Ayala, Q. Cui, K. Morokuma, P. Salvador, J.J. Dannenberg, D.K. Malick, A.D. Rabuck, K. Raghavachari, J.B. Foresman, J. Cioslowski, J.V. Ortiz, A.G. Baboul, B.B. Stefanov, G. Liu, A. Liashenko, P. Piskorz, I. Komaromi, R. Gomperts, R.L. Martin, D.J. Fox, T. Keith, M.A. Al-Laham, C.Y. Peng, A. Nanayakkara, M. Challacombe, P.M.W. Gill, B.G. Johnson, W. Chen, M.W. Wong, J.L. Andres, C. Gonzalez, M. Head-Gordon, E.S. Replogle, J.A. Pople, Pittsburgh PA, 2001.
[24] S.F. Boys, Proc. R. Soc. Lond. A 200 (1950) 542–554.
[25] M.L. Munzarova, M. Kaupp, J. Phys. Chem. B 105 (2001) 12644–12652.
[26] M. Munzarova, M. Kaupp, J. Phys. Chem. A 103 (1999) 9966–9983.
[27] M.L. Munzarova, P. Kubacek, M. Kaupp, J. Am. Chem. Soc. 122 (2000) 11900–11913.
[28] V. Barone, Chem. Phys. Lett. 226 (1994) 392–398.
[29] A.D. Becke, Phys. Rev. A (1988) 3098–3100.
[30] C. Lee, W. Yang, R.G. Parr, Phys. Rev. B 37 (1988) 785–789.
[31] B. Miehlich, A. Savin, H. Stall, H. Preuss, Chem. Phys. Lett. 157 (1989) 200–206.
[32] S.H. Vosko, L. Wilk, M. Nusair, Can. J. Phys. 58 (1980) 1200.
[33] J.P. Perdew, Phys. Rev. B 33 (1986) 8822–8824.
[34] J.P. Perdew, K. Burke, Y. Wang, Phys. Rev. B 54 (1996) 16533–16539.
[35] J.P. Perdew, J.A. Chevary, S.H. Vosko, K.A. Jackson, M.R. Pederson, D.J. Singh, C. Fiolhais, Phys. Rev. B 46 (1992) 6671–6687.
[36] J.P. Perdew, J.A. Chevary, S.H. Vosko, K.A. Jackson, M.R. Pederson, D.J. Singh, C. Fiolhais, Phys. Rev. B 48 (1993) 4978.
[37] E.J. Baerends, D.E. Ellis, P. Ros, Chem. Phys. 2 (1973) 41–51.
[38] L. Versluis, T. Ziegler, J. Chem. Phys. 88 (1988) 322–328.
[39] G. Te Velde, E.J. Baerends, J. Comput. Phys. 99 (1992) 84–98.
[40] A.D. Becke, J. Chem. Phys. 98 (1993) 5648–5652.
[41] A. Frisch, M.J. Frisch, Gaussian98 User's Reference, vol. 6.0, Pittsburgh, PA, 1998.
[42] A. Schafer, H. Horn, R. Ahlrichs, J. Chem. Phys. 97 (1992) 2571–2577.
[43] A.C. Saladino, S.C. Larsen, J. Phys. Chem. A 107 (2003) 1872–1878.
[44] T.S. Smith II, C.A. Root, J.W. Kampf, P.G. Rasmussen, V.L. Pecoraro, J. Am. Chem. Soc. 122 (2000) 767–775.
[45] C.R. Cornman, K.M. Geiser-Bush, S.P. Rowley, P.D. Boyle, Inorg. Chem. 36 (1997) 6401–6408.
[46] C.F. Mulks, B. Kirste, H. van Willigen, J. Am. Chem. Soc. 104 (1982) 5906–5911.
[47] A.C. Saladino, S.C. Larsen, J. Phys. Chem. A 106 (2002) 10444–10451.
[48] A.C. Saladino, S.C. Larsen, J. Phys. Chem. A 107 (2003) 5583–5587.
[49] S.A. Dikanov, C. Burgard, J. Huttermann, Chem. Phys. Lett. 212 (1993) 493–498.
[50] S.S. Eaton, J. Dubach, K.M. More, G.R. Eaton, G. Thurman, D.R. Ambruso, J. Biol. Chem. 264 (1989) 4776–4781.
[51] G.J. Gerfen, P.A. Hanna, N.D. Chasteen, D.J. Singel, J. Am. Chem. Soc. 113 (1991) 9513–9519.
[52] S.C. Larsen, D.J. Singel, J. Phys. Chem. 96 (1992) 9007–9013.
[53] E.J. Reijere, A.M. Tyryshkin, S.A. Dikanov, Magn. Reson. 131 (1998) 295–309.
[54] E.J. Riejerse, J. Shane, E. de Boer, D. Collison (Eds.), ESEEM of Nitrogen Coordinated Oxo-Vanadium(IV) Complexes, World Scientific Publishers, Singapore City, 1989.
[55] D. Mustafi, M.W. Makinen, Inorg. Chem. 27 (1988) 3360–3368.
[56] H. van Willigen, J. Magn. Reson. 39 (1980) 37–46.
[57] S.C. Larsen, J. Phys. Chem. A 105 (2001) 4563–4573.
[58] N.M. Atherton, J.F. Shackleton, Mol. Phys. 39 (1980) 1471–1485.
[59] A.C. Saladino, S.C. Larsen, J. Phys. Chem. A 107 (2003) 4735–4740.
[60] K. Fukui, H. Ohya-Nishiguchi, H. Kamada, Inorg. Chem. 36 (1997) 5518–5529.
[61] R. LoBrutto, B.J. Hamstra, G.J. Colpas, V.L. Pecoraro, W.D. Frasch, J. Am. Chem. Soc. 120 (1998) 4410–4416.
[62] C.P. Scholes, K.M. Falkowski, S. Chen, J. Bank, J. Am. Chem. Soc. 108 (1986) 1660–1671.
[63] K. Fukui, H. Ohya-Nishiguchi, H. Kamada, J. Phys. Chem. 97 (1993) 11858–11860.
[64] R.S. Magliozzo, J. Peisach, Biochemistry 32 (1993) 8446–8456.
[65] S.C. Larsen, D.J. Singel, J. Phys. Chem. 96 (1992) 10594–10597.
[66] C.V. Grant, W. Cope, J.A. Ball, G.G. Maresch, B.J. Gaffney, W. Fink, R.D. Britt, J. Phys. Chem. B 103 (1999) 10627–10631.
[67] M. Torrent, D.G. Musaev, K. Morokuma, S.C. Ke, K. Warncke, J. Phys. Chem. B 103 (1999) 8618–8627.
[68] B.I. Whittington, J.R. Anderson, J. Phys. Chem. 97 (1993) 1032–1041.
[69] T. Blasco, L. Fernandez, A. Martinez-Arias, M. Sanchez-Sanchez, P. Conception, J.M.L. Nieto, Microporous Mesoporous Mater. 39 (2000) 219–228.
[70] M. Petras, B. Wichterlova, J. Phys. Chem. 96 (1992) 1805–1809.
[71] M. Wark, A. Bruckner, T. Liese, W. Grunert, J. Catal. 175 (1998) 48–61.
[72] H. Berndt, A. Martin, A. Bruckner, E. Schreier, D. Muller, H. Kosslick, G.-U. Wolf, B. Lucke, J. Catal. 191 (2000) 384–400.
[73] P.J. Carl, S.L. Isley, S.C. Larsen, J. Phys. Chem. B 105 (2001) 4563–4573.
[74] S.S. Eaton, G.R. Eaton, in: N.D. Chasteen (Ed.), Vanadium in Biological Systems, Kluwer Academic Publishers, Dordrecht, 1990 , pp. 199–222.
[75] S.S. Eaton, J. Dubach, K.M. More, G.R. Eaton, G. Thurman, D.R. Ambruso, J. Biol. Chem. 264 (1989) 4776–4781.
[76] N.D. Chasteen, in: A. Sigel (Ed.), Vanadium and Its Role in Life, vol. 31, M. Decker, New York, 1995, pp. 231–247.
[77] B.J. Hamstra, A.L.P. Houseman, G.J. Colpas, J.W. Kampf, R. LoBrottu, W.D. Frasch, V.L. Pecoraro, Inorg. Chem. 36 (1997) 4866–4874.
[78] S.A. Dikanov, A.M. Tyryshkin, J. Hutterman, R. Bogumil, H.J. Witzel, J. Am. Chem. Soc. 117 (1995).
[79] E. de Boer, C.P. Keijzers, E.J. Reijerse, D. Collison, C.D. Garner, R. Wever, FEBS Lett. 235 (1988) 93–97.

[80] J. Petersen, T.R. Hawkes, D.J. Lowe, J. Am. Chem. Soc. 120 (1998) 10978–10979.
[81] J. Petersen, T.R. Hawkes, D.J. Lowe, J. Inorg. Biochem. 80 (2000) 161–168.
[82] H. van Willigen, T.K. Chandrashekar, J. Am. Chem. Soc. 105 (1983) 4232–4235.
[83] C.F. Mulks, B. Kirste, H. van Willigen, J. Am. Chem. Soc. 104 (1982) 5906–5911.
[84] C.F. Mulks, H. van Willigen, J. Phys. Chem. 85 (1981) 1220–1224.
[85] M.W. Anderson, L. Kevan, J. Phys. Chem. 91 (1987) 4174–4179.
[86] D. Goldfarb, L. Kevan, J. Am. Chem. Soc. 109 (1987) 2303–2311.
[87] C.E. Sass, L. Kevan, J. Phys. Chem. 93 (1989) 7856–7859.
[88] G.-D. Lei, L. Kevan, J. Phys. Chem. 94 (1990) 6384–6390.
[89] J.-S. Yu, L. Kevan, J. Phys. Chem. 94 (1990) 7620–7627.
[90] L. Kevan, J.-S. Yu, Research on Chemical Intermediates, vol. 15, Elsevier Science Publishers B.V., Amsterdam, 1991, pp. 67–80.
[91] G.-D. Lei, L. Kevan, J. Phys. Chem. 95 (1991) 4506–4514.
[92] C. Finel, L. Kevan, J. Chem. Soc. Faraday Trans. 89 (1993) 2559–2565.
[93] Z. Luan, J. Xu, H. He, J. Klinowski, L. Kevan, J. Phys. Chem. 100 (1996) 19595–19602.
[94] A.M. Prakash, L. Kevan, J. Phys. Chem. B 103 (1999) 2214–2222.
[95] L. Kevan, A.M. Prakash, J. Phys. Chem. B 104 (2000) 6860–6868.
[96] P. Hofer, A. Grupp, H. Nebenfuhr, M. Mehring, Chem. Phys. Lett. 132 (1986) 279–282.
[97] P.J. Carl, D.E.W. Vaughan, D. Goldfarb, J. Phys. Chem. B 106 (2002) 5428–5437.
[98] J. Zhang, P.J. Carl, H. Zimmermann, D. Goldfarb, J. Phys. Chem. B 106 (2002) 5382–5389.
[99] S.A. Dikanov, B.D. Liboiron, C. Orvig, J. Am. Chem. Soc. 124 (2002) 2969–2977.
[100] C. Buy, T. Matsui, S. Andrianambinintsoa, C. Sigalat, G. Girault, J. Zimmermann, Biochemistry 35 (1996) 14281–14293.
[101] K. Fukui, H. Ohya-Nishiguchi, H. Kamada, Inorg. Chem. 36 (1997) 5518–5529.
[102] S.A. Dikanov, M.K. Bowman, J. Magn. Reson. 116 (1995) 125–128.
[103] R.I. Samooilova, S.A. Dikanov, A.V. Fionov, A.M. Tyryshkin, E.V. Lunina, M.K. Bowman, J. Phys. Chem. 100 (1996) 17621–17629.
[104] A. Schweiger, G. Jeschke, Principles of pulse electron paramagnetic resonance, Oxford University Press, New York, 2001.
[105] J. Woodworth, M.K. Bowman, S.C. Larsen, J. Phys. Chem. B 108 (2004) 16128–16134.
[106] F. Neese, J. Phys. Chem. A. 105 (2001) 4290–4299.
[107] M. Munzarova, M. Kaupp, J. Phys. Chem. A 103 (1999) 9966–9983.
[108] N.D. Yordanov, M. Stankova, D. Shopov, Chem. Phys. Lett. 39 (1976) 174–176.
[109] F.A. Walker, H. Sigel, D.B. McCormick, Inorg. Chem. 11 (1972) 2756–2763.
[110] I. Adato, I. Eliezer, J. Chem. Phys. 54 (1971) 1472–1476.
[111] H.C. Allen, M.I. Mandrioli, J.W. Becker, J. Chem. Phys. 56 (1972) 997–999.